



HAL
open science

Influence of Climate-Forcing Frequency on Hillslope Response

V. Godard, G. Tucker

► **To cite this version:**

V. Godard, G. Tucker. Influence of Climate-Forcing Frequency on Hillslope Response. *Geophysical Research Letters*, 2021, 48 (18), pp.e2021GL094305. 10.1029/2021GL094305 . hal-03347189

HAL Id: hal-03347189

<https://amu.hal.science/hal-03347189>

Submitted on 17 Sep 2021

HAL is a multi-disciplinary open access archive for the deposit and dissemination of scientific research documents, whether they are published or not. The documents may come from teaching and research institutions in France or abroad, or from public or private research centers.

L'archive ouverte pluridisciplinaire **HAL**, est destinée au dépôt et à la diffusion de documents scientifiques de niveau recherche, publiés ou non, émanant des établissements d'enseignement et de recherche français ou étrangers, des laboratoires publics ou privés.

Influence of climate-forcing frequency on hillslope response

V. Godard^{1,2,*} & G. E. Tucker^{3,4}

September 16, 2021

¹Aix-Marseille Univ, CNRS, IRD, INRAE, Coll France, CEREGE, Aix-en-Provence, France

²Institut Universitaire de France (IUF), Paris, France

³Cooperative Institute for Research in Environmental Sciences (CIRES), University of Colorado, Boulder, CO, USA

⁴Department of Geological Sciences, University of Colorado, Boulder, CO, USA

* Corresponding author : godard@cerege.fr

Published in Godard, V., & Tucker, G. E. (2021). Influence of climate-forcing frequency on hillslope response. *Geophysical Research Letters*, 48, e2021GL094305. <https://doi.org/10.1029/2021GL094305>

Abstract

Assessing rivers' and hillslopes' sensitivity to external forcing is paramount to understand landscape evolution, in particular as a response to Quaternary climate changes. River networks are usually considered to be the main conveyors of environmental signals, such as changes in precipitation, temperature, or baselevel. Yet because hillslopes provide the source of sediment for river networks, their response to environmental change also modulate landscape dynamics. In order to characterize such behavior we analyse the response times of a transport-limited hillslope. We use simple numerical models of denudation to study hillslope responses to oscillatory forcing and understand their filtering effects on environmental signals. Modifications in the frequency of climate oscillation, such as the change that occurred at the Mid-Pleistocene Transition, can significantly modulate hillslope sediment-flux response. We infer a wide range of hillslope responses, ranging from negligible change over the full range of climate-forcing frequencies, to a significant filtering of long-period signals.

26 Plain language summary

27 Landscapes are constituted of hillslopes and rivers where different types of erosion and sediment
28 transport processes take place. Due to their large extent, river networks are an important driver of
29 global landscape response to climatic or tectonic changes. Hillslopes have smaller dimensions but
30 are also where most sediment production occurs and for that reason it is important to have a good
31 understanding of how they respond to perturbations. We use simple numerical models of hillslope
32 evolution to study the influence of oscillating changes of either the efficiency of sediment transport
33 across the hillslope or the rate of channel downcutting at its base. Our results indicates that the
34 period of oscillations for these perturbations controls the amplitude of the sediment flux response
35 out of the hillslope, and provide a framework to understand how this landscape component reacts
36 to climatic cycles such as the glacial/inter-glacial oscillations of the Quaternary. For example, a
37 major change occurred 800 ka ago with a shift in climate oscillation from 40 ka to 100 ka period.
38 Our models suggest that in some landscapes this change in period alone could have induced a
39 significant decrease in the amplitude of hillslope sediment flux response.

40 1 Introduction

41 Landscapes evolve in response to changes in their climatic and tectonic boundary conditions. River
42 networks are usually considered to be the main agents that transmit the effects of such external
43 forcing across landscapes. Due to their dominance in terms of area covered at the Earth's surface,
44 most weathering and sediment production occurs on hillslopes. Geomorphologists sometimes as-
45 sume that the erosion rate on hillslopes closely follows the pace imposed by channel downcutting
46 at their feet [e.g. [Ouimet et al., 2009](#)]. However, several studies have highlighted the potential for
47 a more complex behavior of hillslopes, suggesting that landscape response depends on the nature
48 of the coupling between channels and hillslopes and on the intrinsic dynamics of hillslopes and
49 their response timescales [e.g. [Langston et al., 2015](#); [Romans et al., 2016](#); [Watkins et al., 2018](#);
50 [Clubb et al., 2020](#)]. The hypothesis that hillslope sediment flux depends linearly on topographic
51 gradient, which underpins the diffusion theory of soil-mantled hillslope evolution, has provided
52 a simple and robust framework for understanding their behavior [[Gilbert, 1909](#); [Culling, 1960](#)].
53 However, a growing body of evidence points to a nonlinear relationship between sediment flux
54 and hillslope gradient [[Andrews and Bucknam, 1987](#); [Roering et al., 1999](#); [Tucker and Bradley,](#)
55 [2010](#); [Furbish and Roering, 2013](#); [Doane et al., 2018](#)], which complicates the hillslope response to

56 external forcing and its relationship with the fluvial network. Forcing factors acting on landscapes
57 can be classified into two broad categories [Mudd, 2016]. Climate acts directly as a Top-Down
58 (TD) forcing, producing changes in surface runoff and vegetation cover, which modulate sediment
59 transport efficiency along hillslopes. Bottom-Up (BU) forcing, resulting from changes in the base-
60 level fall rate at the toe of the hillslope, is associated with incision or aggradation in the channel,
61 and can be controlled by any factor impacting the baselevel, such as climate, tectonics, eustatic
62 variations, or auto-cyclic processes.

63 The response time of hillslopes has been intensively studied and characterized under these
64 various types of forcing [Fernandes and Dietrich, 1997; Roering et al., 2001]. It is less clear how
65 this response time interacts with the time characteristics of the input forcing, in particular when
66 dealing with periodic signals associated with climatic variability. Several recent studies focusing
67 on the fluvial domain have highlighted the sensitivity to periodic climatic fluctuations and the
68 importance of their frequency content [Simpson and Castelltort, 2012; Godard et al., 2013; Braun
69 et al., 2015]. The response of the hillslope domain to such forcing has received less attention.
70 Diffusive processes are usually considered to have a strong buffering effect on environmental signals
71 [e.g. Godard et al., 2013], but the signature of more complex hillslope behavior remains to be clearly
72 characterized. From gently rolling hillslopes in low-relief landscapes to near-threshold slopes in
73 actively uplifting areas, hillslopes can present a variety of morphologies, and understanding their
74 importance for landscape evolution requires assessing which types of hillslopes, characterized by
75 a given relief or erosion regime, are most sensitive to the different types of forcing factors.

76 Here, we study the response of hillslopes to periodic variations in climatic and tectonic (base-
77 level) boundary conditions, with a specific focus on the implication of the nonlinear relationship
78 between sediment flux and gradient. We summarize the existing framework used to formulate hill-
79 slope evolution, and its relationship with response time and topographic metrics. We then assess
80 the controls of baselevel fall (here “uplift”) rate and transport coefficient on hillslope response. We
81 specifically study the relationship between the forcing period and the response time of hillslopes,
82 as set by length, uplift rate, and transport efficiency, and discuss the implications for landscape
83 dynamics.

84 **2 Theoretical background**

85 We present here the theoretical formulation for hillslope erosion and sediment flux, and the mod-
86 eling approaches used in this study. Mass conservation applied to 1D hillslope evolution can be

87 expressed as,

$$\frac{\partial z}{\partial t} + \frac{\partial q}{\partial x} = \beta U, \quad (1)$$

88 where z is land surface elevation, t time, q sediment flux ($[L^2T^{-1}]$), β the rock-to-regolith density
 89 ratio, and U the rate of rock uplift relative to baselevel at the foot of the hillslope ($[LT^{-1}]$).
 90 Equation 1 can be combined with a Geomorphic Transport Law [GTL, [Dietrich et al., 2003](#)],
 91 describing sediment flux q over a hillslope. A widely used transport law for soil-mantled hillslopes
 92 [[Roering et al., 1999, 2007](#)] expresses the flux q as a nonlinear function of local slope gradient,

$$q = \frac{-K(\partial z/\partial x)}{1 - [(\partial z/\partial x)/S_c]^2}, \quad (2)$$

93 where K is a transport coefficient ($[L^2T^{-1}]$) and S_c a critical hillslope gradient ($[L/L]$) [[Roering](#)
 94 [et al., 1999](#)]. This expression applies only for $|\partial z/\partial x| < S_c$. The transport law (equation 2) implies
 95 that the degree of nonlinearity in the relationship between gradient and sediment flux varies with
 96 the gradient itself. For our analysis, it is useful to quantify this degree of nonlinearity by separating
 97 the total flux into linear and nonlinear components. Doing so starts with the observation that
 98 in gently sloping parts of the landscape, such as areas close to the hilltops, the sediment flux is
 99 linearly related to topographic gradient as $q_l = -K\partial z/\partial x$. As shown by [Roering et al. \[2001\]](#), the
 100 total flux q can be expressed as the sum of a linear q_l and a nonlinear q_{nl} component,

$$q = q_l + q_{nl} = K \frac{\partial z}{\partial x} + \frac{K \frac{\partial z}{\partial x} \left(\frac{\partial z/\partial x}{S_c} \right)^2}{1 - \left(\frac{\partial z/\partial x}{S_c} \right)^2}. \quad (3)$$

101 Substituting equation 2 into 1 yields a landscape evolution model describing the evolution of
 102 hillslope profile topography $z(x, t)$ through space and time,

$$\frac{\partial z}{\partial t} - K \frac{\partial^2 z}{\partial x^2} \frac{1 + \left(\frac{\partial z/\partial x}{S_c} \right)^2}{\left(1 - \left(\frac{\partial z/\partial x}{S_c} \right)^2 \right)^2} = \beta U. \quad (4)$$

103 We solve equation 4 using the implicit method proposed by [Perron \[2011\]](#). Starting from a steady-
 104 state topography we submit the hillslope to time variations in either K or U , parameterized with
 105 sinusoidal functions,

$$K(t) = K_0 \left(1 + a \sin \left(\frac{2\pi t}{T} \right) \right), \quad U(t) = U_0 \left(1 + a \sin \left(\frac{2\pi t}{T} \right) \right). \quad (5)$$

106 K_0 and U_0 are the average values of K and U , respectively, a is a factor controlling the amplitude of
 107 the forcing, and T is the oscillation period. The reference parameter values used in our simulations
 108 are listed in Table S1.

109 Under steady conditions ($\partial z/\partial t = 0$) equation 4 can be integrated to yield the steady-state
 110 topographic profile [Roering et al., 2001],

$$z(x) = \frac{KS_c^2}{2\beta U} \left(\ln \left(\frac{1}{2} \sqrt{1 + \left(\frac{2\beta U x}{KS_c} \right)^2} + \frac{1}{2} \right) - \sqrt{1 + \left(\frac{2\beta U x}{KS_c} \right)^2} + 1 \right), \quad (6)$$

111 with L as the hillslope length (horizontal distance from hilltop to channel). It is useful to define
 112 a reference erosion rate [Roering et al., 2007] as,

$$E_R = \frac{KS_c}{2L\beta}, \quad (7)$$

113 This reference value provides a way to normalize steady-state erosion rate $E = U$ into its non-
 114 dimensional equivalent as,

$$E^* = \frac{2L\beta U}{KS_c}. \quad (8)$$

115 At steady state, and in the vicinity of hilltops, where topographic gradient is small ($\partial z/\partial x \ll S_c$),
 116 equation 4 simplifies to,

$$U = -\frac{KC_{HT}}{\beta}, \quad (9)$$

117 where hilltop curvature C_{HT} is the second derivative of topography. Combining equations 8 and
 118 9 yields a form of E^* that can be calculated directly from topographic data without needing to
 119 know K [Roering et al., 2007; Hurst et al., 2012],

$$E^* = \frac{2C_{HT}L}{S_c}. \quad (10)$$

120 In order to assess the relative non-linear contribution to the sediment flux, Roering et al. [2001]
 121 introduced the ratio Ψ of the two components,

$$\Psi = \frac{q_{nl}}{q_l} = \frac{\left(\frac{\partial z/\partial x}{S_c} \right)^2}{1 - \left(\frac{\partial z/\partial x}{S_c} \right)^2}. \quad (11)$$

122 Following Roering et al. [2001], and using equation 6, we evaluate this ratio at the base of the

123 hillslope,

$$\Psi_L = \Psi(x = L) = \frac{\left(\frac{S_c}{2\beta UL} \left(-K + \sqrt{K^2 + \left(\frac{2\beta UL}{S_c}\right)^2}\right)\right)^2}{1 - \left(\frac{S_c}{2\beta UL} \left(-K + \sqrt{K^2 + \left(\frac{2\beta UL}{S_c}\right)^2}\right)\right)^2}, \quad (12)$$

124 and we use their definition of an exponential equilibrium adjustment timescale for sediment flux
125 or hillslope morphology calculated as,

$$\tau = \frac{AL^2}{K(1 + \Psi_L)^B}. \quad (13)$$

126 The parameters $A = 0.405$ and $B = 1.74$ were calibrated by [Roering et al. \[2001\]](#) over a range
127 of Ψ_L values reflecting a wide range of environmental conditions and using numerical models for
128 hillslope evolution based on the same physical principles as the one we use here. Substituting
129 equation 8 into 12 yields,

$$\Psi_L = \frac{1}{2}\sqrt{1 + E^{*2}} - \frac{1}{2} \quad (14)$$

130 The non-dimensional framework for hillslope morphology analysis introduced by [Roering et al.](#)
131 [\[2007\]](#) provides a way to reduce erosion dynamics to non-dimensional erosion rates E^* (equation 8),
132 which can be computed on the basis of measurable hillslope morphological characteristics (equation
133 10), such as length and hilltop curvature [[Grieve et al., 2016](#)]. Equation 14 describes the connection
134 between E^* , which can be measured from topographic data, and the degree of nonlinearity of the
135 sediment flux (Ψ_L). In order to compare theoretical predictions of hillslope behavior with actual
136 landscapes, we select case studies for which landscape denudation rates have been constrained
137 with terrestrial cosmogenic nuclides, and where hillslope-scale morphological properties such as
138 hilltop curvature C_{HT} and hillslope length L have been determined using methods similar to those
139 proposed by [Hurst et al. \[2012\]](#) and [Grieve et al. \[2016\]](#) using high resolution topographic data
140 (Figure 1 and Table S2). The topographic data enable calculation of E^* for these sites (equation
141 10), and the cosmogenic data constrain the value of the baselevel parameter U . We also use the
142 global compilation of hillslope transport coefficients by [Richardson et al. \[2019\]](#) and denudation
143 rates by [Codilean et al. \[2018\]](#) to put the inferred hillslope behavior into a broader context.

144 3 Results

145 3.1 Controls on response time

146 Low values (< 0.1) of the nonlinear transport ratio Ψ_L (equation 12) correspond to hillslopes
147 in the linear regime (Figure 1), where response times are insensitive to changes in uplift rate
148 and larger than 100 ka, for observed values of the transport coefficient [Richardson et al., 2019].
149 Conversely, high Ψ_L values (> 1) are associated with dominant contributions of nonlinear fluxes,
150 a situation where response times are controlled by both transport coefficient and uplift rate and
151 where response times are less than 100 ka, except for very low K values. Intermediate Ψ_L values
152 (0.1-1) correspond to a transitional regime, with a drastic modification of the sensitivity of τ with
153 respect to U and K . All investigated settings display $\Psi_L > 1$, except the Southeastern Australian
154 Escarpment (A1 and A2), and thus their dynamics involve significant nonlinear contributions to
155 the hillslope sediment flux, with response times ranging from 10 ka (OR and GM) to several 100s
156 of ka.

157 Very low uplift rates (< 1 m/Ma) imply a near-linear response and $\tau \propto K^{-1}$ (Figure 2A),
158 except for very low transport coefficients. In this regime, the more efficient the sediment transport
159 is to begin with, the faster a hillslope will react to perturbations, all else being equal. On the
160 other hand, for high uplift rates (> 1000 m/Ma) and dominantly nonlinear behavior, τ increases
161 as K^{B-1} over all the range of reported transport coefficient values [Richardson et al., 2019]. This
162 may seem counter-intuitive at first, but it reflects the fact that greater intrinsic transport efficiency
163 also implies a less steep hillslope that is farther below its threshold gradient (in a sense, it gets
164 less extra help from gravity). Intermediate U values (1-100 m/Ma) are characterized by a non-
165 monotonic evolution, with a maximum τ value at the transition between the linear and nonlinear
166 regimes (Figure 2A).

167 There is significant overlap between the arid ($AI < 0.5$) and humid ($AI > 0.5$) subsets in the
168 transport coefficient database of Richardson et al. [2019], with very close modal values (Figure
169 2A). But arid climates' K distribution is skewed toward lower values, with some cases displaying
170 K an order of magnitude lower than the mode of the whole data set. In the nonlinear regime, for
171 a given U , decreasing K by an order of magnitude will yield a similar change in the response time.
172 Conversely, for a given K , an order of magnitude change in U triggers a nearly 100-fold change
173 in the response time. Despite having their K and U spread over almost two orders of magnitude,
174 most investigated case studies are close to the transition between the linear and nonlinear regimes

175 corresponding to the local τ maximum, with the exception of OR, which presents the maximum
 176 Ψ_L value in our dataset and is clearly in the nonlinear regime.

177 We show here that E^* and Ψ_L are related through equation 14, with two distinct regimes
 178 (Figure 2B). The first is a purely linear-diffusive regime, with $\Psi_L \ll 1$, $E^* \ll 1$, and $\Psi_L \propto E^{*2}$.
 179 The second is a nonlinear regime, for $\Psi_L \gg 1$ and $E^* \gg 1$. Here, the rate of increase in Ψ_L with
 180 respect to E^* is less rapid, with $\Psi_L \propto E^*$. For a given K , response time is constant for low E^*
 181 hillslopes, consistently with linear diffusion theory, and it decreases very rapidly with increasing
 182 E^* , as $\tau \propto E^{*-B}$, when moving into the nonlinear domain (dashed brown lines on Figure 2B).
 183 For a given baselevel fall (uplift) rate U (solid brown lines on Figure 2B), the evolution of τ is
 184 non-monotonic, as already observed on Figure 2A. In the linear diffusion regime, τ increases as
 185 E^* and then $\tau \propto E^{*1-B}$ for hillslopes dominated by nonlinear sediment fluxes. Over the range
 186 of U considered here, a local maximum appears at $E^* \sim 2$, coincident with the change in scaling
 187 between E^* and Ψ_L , for Ψ_L between 0.1 and 1.

188 We again observe that the investigated case studies are close to the transition zone between
 189 the two regimes, but mostly on the nonlinear side of that transition, with the exception of the
 190 Southeastern Australian Escarpment (A1 and A2). An increase in U or a decrease in K would
 191 tip them further in the nonlinear domain, with a drop in their response time τ . Conversely, a
 192 decrease in U or an increase in K would bring them closer to the transition, but with only a
 193 limited influence on τ .

194 3.2 Response to oscillatory forcing

195 Here we analyze hillslope response to oscillating Top-Down (K oscillations) or Bottom-Up (U
 196 oscillations) forcing (equations 5). We quantify the response gain, G , as the ratio between the
 197 normalized amplitudes of the output (sediment flux) and input (forcing) signals :

$$G = \frac{\Delta F / F_{ss}}{2a}, \quad (15)$$

198 where ΔF is the peak-to-peak amplitude of the sediment flux response, F_{ss} is the steady state
 199 flux, used for normalization of the output signal, and $2a$ is the peak-to-peak amplitude factor
 200 of the input forcing (equations 5 and Figures S1 and S2). Gain represents the strength of the
 201 response relative to that of forcing. A one-to-one relationship between forcing and response would
 202 correspond to $G = 1$; if $G < 1$ the response is damped, and if $G > 1$ it is amplified.

203 For Bottom-Up (U) fluctuations we observe that gain is near zero at high frequencies and
204 moves toward 1 at low frequencies, whereas the evolution is the opposite in the Top-Down (K)
205 case (Figure 3). Short-term fluctuations in K instantaneously modulate the sediment flux without
206 time for morphological adjustment of the hillslope. On the other hand, longer timescale variations
207 in K are slow enough to allow the hillslope to adjust its morphology and remain close to steady
208 state, with a constant sediment flux matching the constant uplift rate and a gain close to 0. In
209 the Bottom-Up case, high-frequency oscillations in U are too fast to be propagated upslope and
210 remain a very local effect at the base of the hillslope, which does not induce a global response.
211 High-frequency U oscillations therefore yield a gain close to 0. On the other hand, if the forcing
212 period is longer than the hillslope response time, upslope propagation can trigger a global response
213 in terms of sediment flux variation.

214 Overall, decreasing K (Figure 3A, dotted curves) or increasing U (Figure 3B, dashed curves)
215 by a factor of 10 with respect to the reference model moves the hillslope toward the nonlinear
216 regime, with a strong decrease in the response time. For both types of forcing a decrease in K
217 (Figure 3A, dotted curves) leads to an earlier transition when increasing the forcing period due
218 to the corresponding shorter response time (indicated by the dotted vertical lines on Figure 3).
219 Interestingly, increasing K by a factor 10 (Figure 3A, dashed curves) does not substantially change
220 the response curves (for either type of forcing), which is consistent with the similar response times
221 for the reference and $K \times 10$ models (solid and dashed vertical lines respectively on Figure 3). The
222 response time in the $K \times 10$ model is actually slightly shorter than the reference case (Figures 1 and
223 2A), as the evolution of τ is non-monotonic, with a maximum in response time at the transition
224 between the linear and nonlinear regimes; the reference and $K \times 10$ cases are located on both
225 sides of this transition, and have relatively similar response times. Changes in the background
226 uplift rate (Figure 3B) are similarly shifting the response to the variations in the forcing period,
227 consistently with the effect of U on the response time of the hillslope (Figure 1). The amplitude
228 of this shift appears to be larger than what is induced by the variations in K (Figure 3A).

229 We now consider response curves to Top-Down forcing (time variations in K) using reference
230 values of K from the observations compiled by Richardson et al. [2019] (Figure 4A). In order to
231 further analyze the role of climatic context we first use mean K values for the whole dataset,
232 and then for arid ($AI < 0.5$) and humid subsets (solid lines on Figure 4A). Due to the considerable
233 overlap between the distributions, the response curves are very similar. We also test the response
234 for the lowest quartile Q_1 of the arid subset ($AI < 0.5$) and the highest quartile Q_3 of the humid

subset ($AI > 0.5$). In this case the two climatically contrasting settings yield distinct response curves, with gain differences up to 0.2 for a given forcing frequency.

We can also analyze the impact of changes in the climatic forcing frequency, such as the shift occurring at the Mid-Pleistocene Transition (MPT), when the dominant period of oscillations, as recorded by marine oxygen isotopes, shifted from the orbital obliquity period (40 ka) to the eccentricity period (100 ka), at ~ 800 ka ago. In the case of Top-Down forcing, such shift in frequency would induce a decrease in response gain. For high- K or low- U settings, where linear diffusion is prevalent, this decrease in gain is < 0.1 , but can be > 0.2 for high- U or low- K situations, when the hillslope behavior is dominated by nonlinear processes. Finally, we calculate the response curves to Top-Down forcing using the parameters compiled for the investigated case studies (Table S2 and Figure 4B). We observe the whole range of responses for this selection of sites, with areas such as the Southeastern Australian Escarpment (A1 and A2) showing high gain, with only a slight decrease over the full range of periods. On the other hand, in settings such as the Gabilan Mesa (GM) or the Oregon Coast Range (OR) gain decreases from ~ 0.9 , down to < 0.2 when increasing the forcing period. When considering the MPT, the frequency shift alone would imply a decrease of ~ 0.2 for the response gain. Overall, the sensitivity of hillslope response to the frequency content of climatic fluctuations appears to be quite different among these different locations.

4 Discussion and conclusions

Our results illustrate a complex hillslope response to various types of forcing, which is controlled by the transition between linear and nonlinear regimes [Roering et al., 2001]. The various combinations of transport coefficient K and relative uplift rate U at the foot of the hillslope set its Ψ_L value and have a complex influence on its dynamics (Figure 1). Parameters describing the morphology of the hillslope, such as nondimensional erosion rate E^* (equation 8), can be expressed as functions of the U/K ratio, such that changing U and K by the same factor does not impact steady state hillslope morphology. Conversely the hillslope response time τ (equation 13) can not be expressed as a function of the U/K ratio, which implies that a given hillslope morphology, as defined by E^* value, can correspond to very different response times. These contrasts can reach almost one order of magnitude, depending on the individual U and K values, as illustrated by the differences in τ despite similar E^* in the VA vs GM or CR vs NC case studies (Figure 2B).

For hillslopes eroding in the 10–100 m/Ma range, the mode of K values from the Richardson

266 [et al. \[2019\]](#) dataset is almost coincident with the local maxima for τ (Figure 2A), implying that
267 moderate climate-driven changes in K will have only a modest impact on the value of τ . The
268 trade-off between U and K in controlling Ψ_L and E^* values is reflected in the position of the local
269 maximum in τ , which occurs at higher K values when U increases. In the nonlinear dominated
270 domain, changing U by an order of magnitude implies a nearly two order of magnitude change in
271 τ , whereas a similar amplitude change in K results only in less than an order of magnitude change
272 in τ (Figure 2A). This importance of changes in U on hillslope response is confirmed by the steep
273 slope of the constant- K curves from Figure 2B (solid brown lines) for $E^* > 1$, as well as by the
274 different impacts on the response curves of orders of magnitude changes in background K and U
275 (Figures 3A vs 3B).

276 The filtering or transmitting behavior of hillslopes with respect to high frequency environmental
277 perturbations depends the values of U and K , as well as on the type of forcing, as Top-Down (TD)
278 and Bottom-Up (BU) forcing are buffered at the opposite ends of the spectrum (Figure 3). For the
279 usual range of K values, hillslopes transmit TD forcing up to period of ~ 100 ka (gain G close to 1),
280 but with a significant lowering of this limit when increasing uplift rates (Figure 3B, blue dashed
281 curve). As a consequence, the sediment flux from near-threshold hillslopes in high-uplift regions
282 appears less likely to be directly modulated by climate over the 10-100 ka range of astronomical
283 forcing frequencies. On the other hand, BU forcing are strongly filtered at short periods (G close
284 to 0) [[Furbish and Fagherazzi, 2001](#)]. Climatic fluctuations can of course act simultaneously as TD
285 and BU-types forcing. Simultaneous changes in vegetation, soil moisture, and runoff generation
286 can potentially lead to complex (but spatially synchronous) modulation of K in the frame of a
287 TD-type forcing [e.g. [Bovy et al., 2016](#)]. The case of vegetation changes when shifting toward drier
288 or wetter climates is known to trigger complex responses across landscapes. Such responses mean
289 that K is not necessarily a simple linear function of mean annual precipitation. For example,
290 transport efficiency may actually increase when a dense and thick forest is replaced with shrubs or
291 grass under a more arid climate [[Pelletier, 2014](#); [Pelletier et al., 2016](#); [Sharma et al., 2021](#)]. Climate
292 changes can also modulate river incision efficiency at the foot of the hillslope as a BU-type forcing,
293 which acts locally and then propagates upslope with progressive adjustments. In our simulations
294 we have separated the two types of forcing in order to isolate their specific properties (Figure
295 3). In many settings it is likely that climatic fluctuations might trigger both types of responses,
296 acting simultaneously on the hillslope, with potential constructive or destructive interactions,
297 depending on the amount of phase offset between the two signals. However, orbitally-controlled

298 climatic forcing operating in the 10-100 ka range is expected to have a limited expression on river
299 profiles [Goren, 2016], which is an additional argument for a limited impact of astronomically
300 tuned BU-type forcing on hillslopes.

301 The response curves for TD-type forcing (Figure 4) show a steep decline over the 10 ka to 1
302 Ma range, implying that the 40 to 100 ka shift associated with the Mid-Pleistocene Transition
303 (MPT) could have triggered a drop in gain up to 0.2 for arid and/or rapidly eroding (i.e., high
304 E^*) landscapes, whereas for wetter or more slowly eroding landscapes (i.e., low E^*) the drop is
305 limited to <0.1 . Overall, a frequency decrease such as the MPT resulted in a significant lowering
306 of the sensitivity of hillslopes to climatically driven oscillations in transport coefficient. The pure
307 frequency shifts considered here are likely to be superimposed on climatically controlled increases
308 or decreases in the long-term average transport coefficient value, resulting in a corresponding
309 transient perturbation of the averaged sediment flux.

310 For Top-Down forcing at glacial-interglacial frequencies, the expected gain ranges from about
311 0.4 to 0.9 (Figure 4A). To understand how this translates into variations in hillslope sediment
312 supply, one needs estimates of the amplitude of climatically modulated variations in K . An
313 analysis of frost-driven creep by Anderson et al. [2013] presented an example in which variations
314 in mean annual temperature similar to those associated with ice-age cycles produced variation in
315 K between 0.005 and 0.04 m^2/y . If one treated this as a sinusoidal variation around the mid-point,
316 the corresponding amplitude would be about ± 0.8 times the mean. Given the above range of gain
317 values, this translates into an amplitude of sediment flux variation between 0.3 and 0.7 times the
318 temporal mean.

319 Conversely, given data on climatically controlled variations in hillslope sediment flux, one
320 could also infer the corresponding variation in K . For example, Hughes et al. [2009] documented a
321 near-doubling increase in flux (0.0012 to 0.0022 m^2/y) in New Zealand associated with vegetation
322 change across the Pleistocene-Holocene transition. If this were treated as sinusoidal oscillations
323 about the midpoint, a flux variation amplitude of about ± 0.3 times the mean with a gain range
324 of 0.4 to 0.9 implies an amplitude of flux variation between about 33% and 74% of the mean flux.
325 This kind of information is valuable for understanding and modeling whole-landscape response to
326 cyclic climate forcing [e.g., Langston and Tucker, 2018].

327 Globally, our results illustrate a complex and frequency-dependent hillslope response to os-
328 cillating boundary conditions. The linear/nonlinear transition implies the potential for complex
329 non-monotonic evolution and a sensitivity to changes in periodicity over Milankovitch time scales,

330 such as the 40 to 100 ka Mid-Pleistocene Transition. As most sediment production occurs on hill-
331 slopes, global-scale analysis of the impact of climate fluctuations on landscapes should integrate
332 the intrinsic hillslope responses to various types of forcing.

333 **Acknowledgements**

334 This research was supported by an IUF fellowship and ANR grant TopoExtreme to VG and NSF
335 grant EAR-1831623 to GT. We thank two anonymous reviewers for their help in improving our
336 manuscript.

337 **Data and code availability**

338 Data used in this study is available through [Codilean et al. \[2018\]](#); [Godard et al. \[2019, 2020\]](#); [Grieve](#)
339 [et al. \[2016\]](#); [Hurst et al. \[2012\]](#); [Richardson et al. \[2019\]](#); [Roering et al. \[2007\]](#). The code used for the
340 modeling are available in the following repository: <https://gitlab.osupytheas.fr/vgodard/geomorphology>

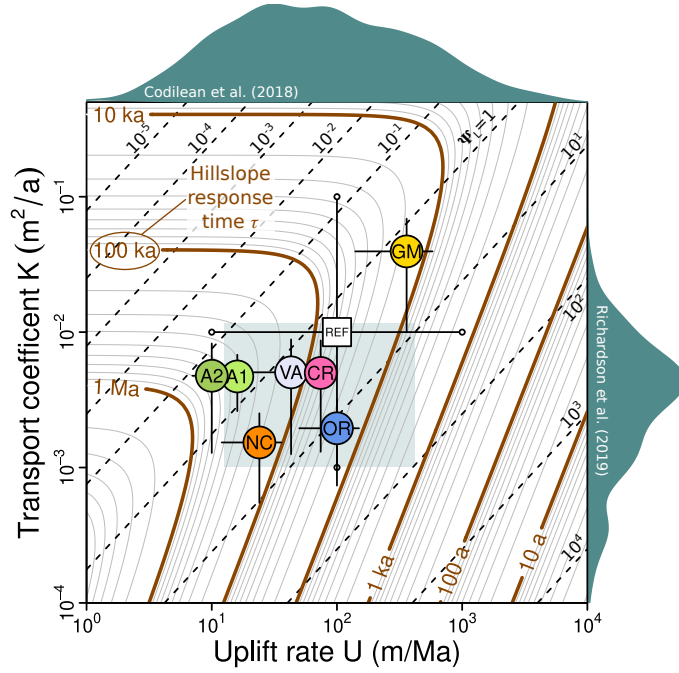


Figure 1: Hillslope response timescale τ (solid contours) [Roering et al., 2001] as a function of transport coefficient K and uplift rate U . Dashed lines correspond to different values of the non-linear transport ratio Ψ_L [Roering et al., 2001]. Kernel Density Estimates for transport coefficient [Richardson et al., 2019] and erosion rate [Codilean et al., 2018] compilations are also plotted in front of the corresponding axes. The light blue rectangle indicates the interquartile range from both datasets. Black white square is the reference K and U values, while small white circles indicate other couples of values tested in figure 3. Colored circles correspond to the case studies presented in the supplementary materials (Table S2). A1 and A2 : Southeastern Australian Escarpment, lowlands and highlands, respectively [Godard et al., 2019]. CR : Cascade ridge, Sierra Nevada, CA [Hurst et al., 2012; Grieve et al., 2016]. GM : Gabilan Mesa, CA [Roering et al., 2007; Grieve et al., 2016]. NC : Coweeta, southern Appalachians, NC [Grieve et al., 2016]. OR : Oregon Coast Range, OR [Roering et al., 2007; Grieve et al., 2016]. VA : Valensole Plateau, Provence, France [Godard et al., 2020].

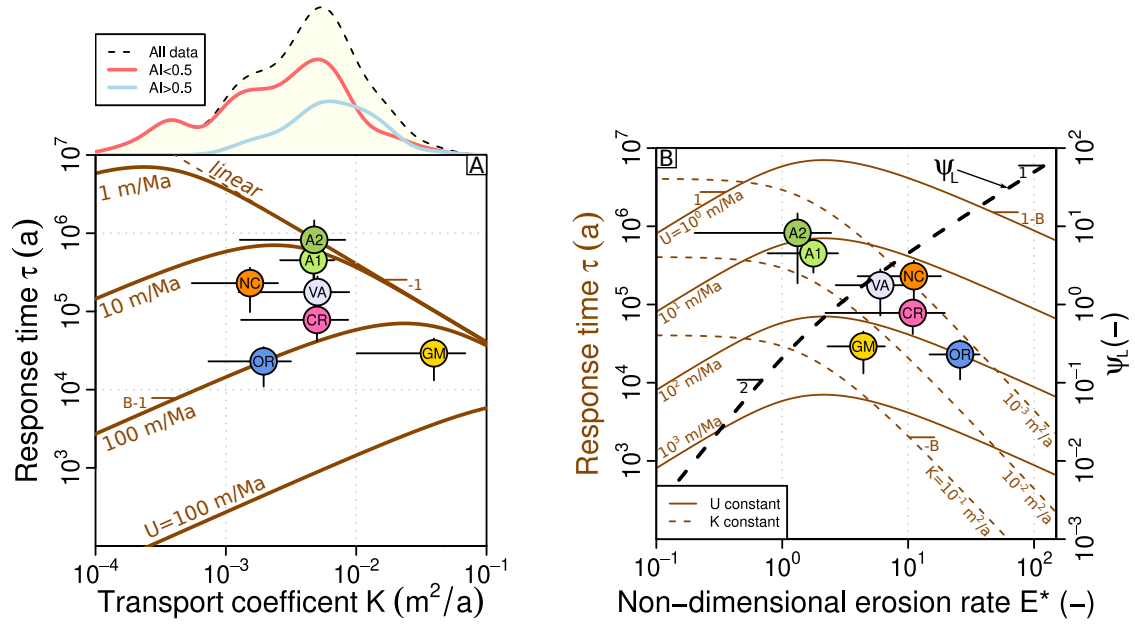


Figure 2: (A) Evolution of response timescale τ [Roering et al., 2001] as a function of transport coefficient K , for different values of uplift rate U . Brown dashed line corresponds to purely linear diffusion ($\Psi_L = 0$ in equation 13). Kernel Density Estimates for transport coefficients compiled by Richardson et al. [2019] are also plotted above the graph. Black dashed line is the whole dataset, whereas red and blue lines correspond to Aridity Index (AI) lower or higher than 0.5, respectively. Colored circles correspond to the case studies presented in the text and on figure 1. Reported slope values correspond to the exponents of asymptotic power law relationships between τ and K . (B) Evolution of hillslope response time τ as a function of non-dimensional erosion rate E^* [Roering et al., 2007], for different constant transport coefficient K (dashed brown lines) or uplift rates U (solid brown lines) values. Dashed black line shows the evolution of the nonlinear transport ratio Ψ_L [Roering et al., 2001] as a function of non-dimensional erosion rate E^* . Colored circles correspond to the case studies presented in figure 1 and supplementary materials. Reported slope values correspond to the exponents of asymptotic power law relationships between either τ and E^* , or Ψ_L and E^* .

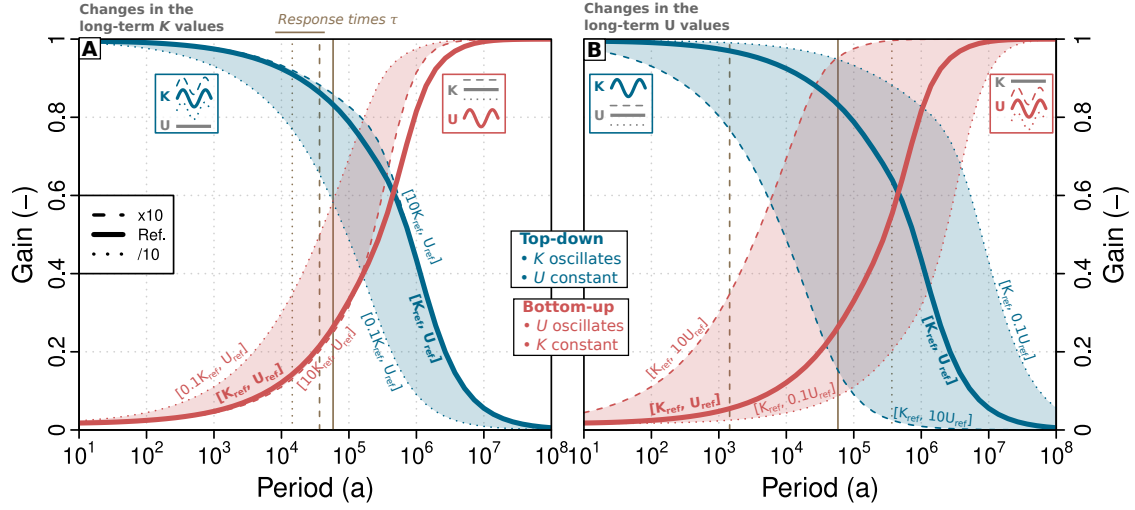


Figure 3: Sensitivity of hillslope sediment flux to oscillation period for Top-Down (K oscillations, blue) and Bottom-Up (U oscillations, red) forcing. The response curves show the evolution of gain, defined as the ratio of the output to input signals normalized amplitudes (equation 15), as a function of the input forcing period. Examples of corresponding time-series are presented on figures S1 and S2. Thick solid lines correspond to reference values for both U and K (100 m/Ma and 0.01 m²/a, respectively, table S1). Dashed and dotted lines corresponds to U_{ref} or $K_{ref} \times 10$ or $\times 0.1$, respectively. See figure 1 for the location of the different combinations in the ($U;K$) plane. Vertical lines (solid, dashed and dotted) indicate the response times (τ) for the corresponding hillslopes (equation 13). (A) Long-term erosion rate is fixed to the reference value $U = 100$ m/Ma (but fluctuates around this value in the Bottom-Up cases). Three values of K are tested (reference, $\times 10$, $\times 0.1$), which in the Top-Down cases (K oscillations) correspond to the average value. (B) Long-term transport coefficient is fixed to the reference value $K = 0.01$ m²/a (but fluctuates around this value in the Top-Down cases). Three values of U are tested (reference, $\times 10$, $\times 0.1$), which in the Bottom-Up cases (U oscillations) correspond to the average value.

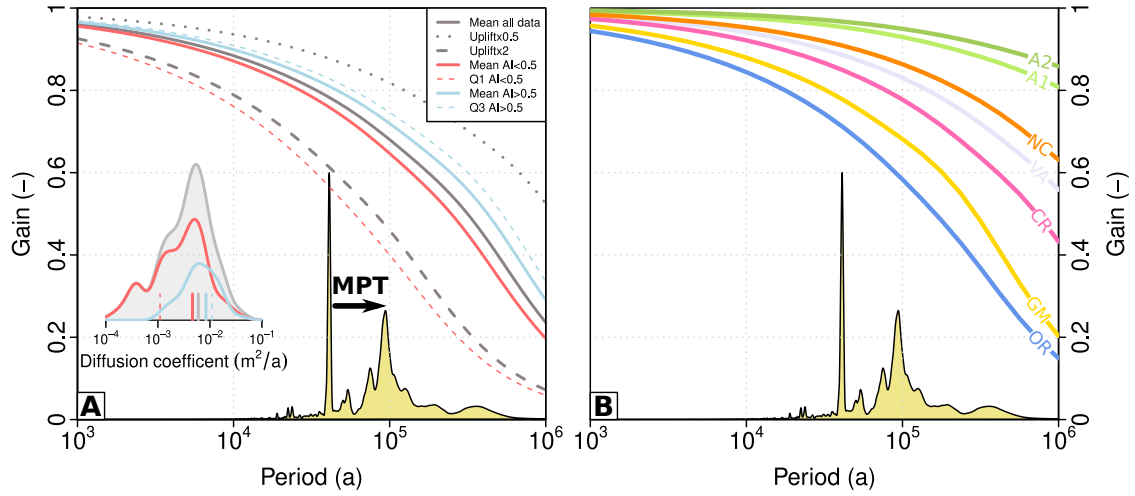


Figure 4: (A) Response curves for Top-Down forcing (figure 3), where the transport coefficient is set to the average values of Richardson et al. [2019] dataset. Dark grey is for all data ($\bar{K} = 59.8$ cm^2/a), whereas red and blue lines correspond to Aridity Index (AI) lower ($\bar{K} = 46.2$ cm^2/a) or higher ($\bar{K} = 83.9$ cm^2/a) than 0.5, respectively. Dashed red and blue lines correspond to first quartile for AI < 0.5 and third quartile for AI > 0.5, respectively. Reference uplift rate value is 100 mm/ka, and other parameters are from table S1. Dashed and dotted gray lines correspond to reference uplift rate multiplied by factors 2 and 0.5, respectively. Yellow curve is the power spectrum density from Lisiecki and Raymo [2005] $\delta^{18}O$ stack (arbitrary units). Black arrow denotes the shift in dominant climatic oscillation period at the Mid-Pleistocene Transition (MPT, 40 ka to 100 ka). (B) Response curves for Top-Down forcing with hillslopes parameters set to the cases studies used here (Table S2). References to labels and colors are the same as figure 1.

References

- Anderson, R. S., Anderson, S. P., and Tucker, G. E. (2013). Rock damage and regolith transport by frost: an example of climate modulation of the geomorphology of the critical zone. *Earth Surface Processes and Landforms*, 38(3):299–316.
- Andrews, D. J. and Bucknam, R. C. (1987). Fitting degradation of shoreline scarps by a nonlinear diffusion model. *Journal of Geophysical Research: Solid Earth*, 92(B12):12857–12867. [_eprint: https://agupubs.onlinelibrary.wiley.com/doi/pdf/10.1029/JB092iB12p12857](https://agupubs.onlinelibrary.wiley.com/doi/pdf/10.1029/JB092iB12p12857).
- Bovy, B., Braun, J., and Demoulin, A. (2016). A new numerical framework for simulating the control of weather and climate on the evolution of soil-mantled hillslopes. *Geomorphology*, 263:99–112.
- Braun, J., Voisin, C., Gurlan, A. T., and Chauvel, C. (2015). Erosional response of an actively uplifting mountain belt to cyclic rainfall variations. *Earth Surface Dynamics*, 3(1):1–14.
- Clubb, F. J., Mudd, S. M., Hurst, M. D., and Grieve, S. W. (2020). Differences in channel and hillslope geometry record a migrating uplift wave at the Mendocino triple junction, California, USA. *Geology*, 48(2):184–188.
- Codilean, A. T., Munack, H., Cohen, T. J., Saktura, W. M., Gray, A., and Mudd, S. M. (2018). OCTOPUS: an open cosmogenic isotope and luminescence database. *Earth System Science Data*, 10(4):2123–2139.
- Culling, W. E. H. (1960). Analytical Theory of Erosion. *The Journal of Geology*, 68(3):336–344.
- Dietrich, W. E., Bellugi, D. G., Sklar, L. S., Stock, J. D., Heimsath, A. M., and Roering, J. J. (2003). Geomorphic transport laws for predicting landscape form and dynamics. In Wilcock, P. R. and Iverson, R. M., editors, *Prediction in Geomorphology*, volume 135, pages 103–132. American Geophysical Union, Washington, D. C. Series Title: Geophysical Monograph Series ISSN: 0065-8448.
- Doane, T. H., Furbish, D. J., Roering, J. J., Schumer, R., and Morgan, D. J. (2018). Nonlocal Sediment Transport on Steep Lateral Moraines, Eastern Sierra Nevada, California, USA. *Journal of Geophysical Research: Earth Surface*, 123(1):187–208.
- Fernandes, N. F. N. and Dietrich, W. W. E. (1997). Hillslope evolution by diffusive processes:

369 The timescale for equilibrium adjustments. *Water Resources Research*, 33(6):1307–1318. ISBN:
370 0043-1397.

371 Furbish, D. J. and Fagherazzi, S. (2001). Stability of creeping soil and implications for hillslope
372 evolution. *Water Resources Research*, 37(10):2607–2618. Publisher: American Geophysical
373 Union.

374 Furbish, D. J. and Roering, J. J. (2013). Sediment disentrainment and the concept of local versus
375 nonlocal transport on hillslopes. *Journal of Geophysical Research: Earth Surface*, 118(2):937–
376 952.

377 Gilbert, G. K. (1909). The convexity of hilltops. *The Journal of Geology*, 17(4):344–350.

378 Godard, V., Dosseto, A., Fleury, J., Bellier, O., Siame, L., and ASTER, T. (2019). Transient land-
379 scape dynamics across the Southeastern Australian Escarpment. *Earth and Planetary Science*
380 *Letters*, 506:397–406. Publisher: Elsevier B.V.

381 Godard, V., Hippolyte, J.-C., Cushing, E., Espurt, N., Fleury, J., Bellier, O., and Ollivier, V.
382 (2020). Hillslope denudation and morphologic response to a rock uplift gradient. *Earth Surface*
383 *Dynamics*, 8(2):221–243.

384 Godard, V., Tucker, G. E., Fisher, G. B., Burbank, D. W., Bookhagen, B., Burch Fisher, G., Bur-
385 bank, D. W., and Bookhagen, B. (2013). Frequency-dependent landscape response to climatic
386 forcing. *Geophysical Research Letters*, 40(5):859–863.

387 Goren, L. (2016). A theoretical model for fluvial channel response time during time-dependent
388 climatic and tectonic forcing and its inverse applications. *Geophysical Research Letters*,
389 43(20):10,753–10,763.

390 Grieve, S. W. D., Mudd, S. M., Hurst, M. D., and Milodowski, D. T. (2016). A nondimensional
391 framework for exploring the relief structure of landscapes. *Earth Surface Dynamics*, 4(2):309–
392 325.

393 Hughes, M. W., Almond, P. C., and Roering, J. J. (2009). Increased sediment transport via
394 bioturbation at the last glacial-interglacial transition. *Geology*, 37(10):919–922.

395 Hurst, M. D., Mudd, S. M., Walcott, R., Attal, M., and Yoo, K. (2012). Using hilltop curvature to
396 derive the spatial distribution of erosion rates. *Journal of Geophysical Research*, 117(F2):F02017.

- 397 Langston, A. L. and Tucker, G. E. (2018). Developing and exploring a theory for the lateral
398 erosion of bedrock channels for use in landscape evolution models. *Earth Surface Dynamics*,
399 6(1):1–27.
- 400 Langston, A. L., Tucker, G. E., and Anderson, R. S. (2015). Interpreting climate-modulated
401 processes of terrace development along the Colorado Front Range using a landscape evolution
402 model. *Journal of Geophysical Research: Earth Surface*, 120(10):2121–2138.
- 403 Lisiecki, L. E. and Raymo, M. E. (2005). A Pliocene-Pleistocene stack of 57 globally distributed
404 benthic d18O records. *Paleoceanography*, 20(1):PA1003. Publisher: American Geophysical
405 Union.
- 406 Mudd, S. M. (2016). Detection of transience in eroding landscapes. *Earth Surface Processes and*
407 *Landforms*, 42(1):24–41. ISBN: 0197-9337.
- 408 Ouimet, W. B., Whipple, K. X., and Granger, D. E. (2009). Beyond threshold hillslopes: Channel
409 adjustment to base-level fall in tectonically active mountain ranges. *Geology*, 37(7):579–582.
410 Publisher: Geological Society of America.
- 411 Pelletier, J. D. (2014). The linkages among hillslope-vegetation changes, elevation, and the timing
412 of late-Quaternary fluvial-system aggradation in the Mojave Desert revisited. *Earth Surface*
413 *Dynamics*, 2(2):455–468. ISBN: 2196-6311.
- 414 Pelletier, J. D., Nichols, M. H., and Nearing, M. A. (2016). The influence of Holocene vegeta-
415 tion changes on topography and erosion rates : A case study at Walnut Gulch Experimental
416 Watershed , Arizona. *Earth Surface Dynamics Discussion*, pages 471–488.
- 417 Perron, J. T. (2011). Numerical methods for nonlinear hillslope transport laws. *Journal of Geo-*
418 *physical Research*, 116(F2):F02021.
- 419 Richardson, P. W., Perron, J. T., and Schurr, N. D. (2019). Influences of climate and life on
420 hillslope sediment transport. *Geology*, 47(5):1–4.
- 421 Roering, J. J., Kirchner, J. W., and Dietrich, W. E. (1999). Evidence for nonlinear, diffusive
422 sediment transport on hillslopes and implications for landscape morphology. *Water Resources*
423 *Research*, 35(3):853–870. Publisher: American Geophysical Union.

- 424 Roering, J. J., Kirchner, J. W., and Dietrich, W. E. (2001). Hillslope evolution by nonlinear,
425 slope-dependent transport: Steady state morphology and equilibrium adjustment timescales.
426 *Journal of Geophysical Research*, 106(B8):16499–16513. ISBN: 0148-0227.
- 427 Roering, J. J., Perron, J. T., and Kirchner, J. W. (2007). Functional relationships between
428 denudation and hillslope form and relief. *Earth and Planetary Science Letters*, 264(1-2):245–
429 258.
- 430 Romans, B. W., Castelltort, S., Covault, J. a., Fildani, A., and Walsh, J. (2016). Environmental
431 signal propagation in sedimentary systems across timescales. *Earth-Science Reviews*. Publisher:
432 Elsevier B.V.
- 433 Sharma, H., Ehlers, T. A., Glotzbach, C., Schmid, M., and Tielbörger, K. (2021). Effect of rock
434 uplift and Milankovitch timescale variations in precipitation and vegetation cover on catchment
435 erosion rates. *Earth Surface Dynamics Discussions*, pages 1–29. Publisher: Copernicus GmbH.
- 436 Simpson, G. and Castelltort, S. (2012). Model shows that rivers transmit high-frequency climate
437 cycles to the sedimentary record. *Geology*, 40(12):1131–1134.
- 438 Tucker, G. E. and Bradley, D. N. (2010). Trouble with diffusion: Reassessing hillslope erosion
439 laws with a particle-based model. *Journal of Geophysical Research*, 115:1–12. ISBN: 0148-0227.
- 440 Watkins, S. E., Whittaker, A. C., Bell, R. E., McNeill, L. C., Gawthorpe, R. L., Brooke, S. A., and
441 Nixon, C. W. (2018). Are landscapes buffered to high-frequency climate change? A comparison
442 of sediment fluxes and depositional volumes in the Corinth Rift, central Greece, over the past
443 130 k.y. *GSA Bulletin*, 131(3-4):372–388.